FORMATION OF THE SOLAR 10830 Å LINE

E. H. AVRETT
Harvard-Smithsonian Center for Astrophysics, 60 Garden Street, Cambridge, MA 02138, U.S.A.
J. M. FONTENLA
The University of Alabama in Huntsville, Huntsville, AL 35899, U.S.A.
and
R. LOESER
Harvard-Smithsonian Center for Astrophysics, 60 Garden Street, Cambridge, MA 02138, U.S.A.

Abstract. One-dimensional hydrostatic-equilibrium models are shown here for faint, average, and bright components of the quiet Sun, and for a plage region, describing in each case how the atmosphere is stratified through the photosphere, chromosphere, and transition region up to a temperature of 10^5 K. The observed coronal line radiation is assumed to be the inward incident radiation at the 10^5 K boundary. This coronal radiation penetrates into the upper chromosphere causing sufficient helium ionization to populate the lower level of the He I 10830 Å line, producing optically-thin absorption of the photospheric continuum at 10830 Å. The amount of absorption, which is proportional to the optical thickness of the upper chromosphere in the 10830 line, depends on 1) the strength of the coronal lines at wavelengths in the He I 504 Å ionizing continuum, and 2) the density and geometrical thickness of the upper chromosphere. The computed 10830 Å line is shown for the four atmospheric models and for three values of the coronal illumination. The calculated off-limb 10830 intensity distribution shows a minimum in the low chromosphere and a maximum at roughly 2000 km above the photosphere, in general agreement with observations, indicating that this is the predominant height of the transition region over most of the solar surface.

Key words: He I 10830 Å – infrared: stars – line: formation – Sun: atmosphere

1. Introduction

In this paper we show how the solar helium 10830 Å line is formed in various model calculations. We use one-dimensional models to represent faint, average, and bright regions of the quiet Sun and to represent a plage region. We treat these components separately, ignoring horizontal interactions, since the horizontal size of the smallest observed features is large compared to the vertical extent of the region in which the spectrum is formed.

Each component model is constructed as follows: in the photosphere and chromosphere we start with an assumed distribution of temperature *vs.* height and use the hydrostatic equilibrium equation to determine the distribution of pressure *vs.* height. A turbulent pressure contribution is included based on the microturbulent velocity inferred from the Doppler widths of lines formed at various heights in excess of thermal Doppler widths. Our models do not include magnetic forces.

We solve the equations of radiative transfer and statistical equilibrium to determine the atomic and molecular number densities and internal radiation intensities, and we use energy-balance equations to determine the temperature distribution in the transition region, as explained below. Then we calculate the emergent spectrum and compare it with solar observations. The differences between the observed and computed spectra are analyzed, and then the assumed temperature distribution is

D. M. Rabin et al. (eds.), Infrared Solar Physics, 35–47.

modified to yield a new computed spectrum that is in closer agreement with the observations. The process is continued until good agreement with available observations is obtained. Thus the observed spectrum "determines" the corresponding temperature distribution.

The observed increase in the brightness temperature of the solar spectrum at far infrared wavelengths, $\lambda > 150$ μm and at ultraviolet wavelengths, $\lambda < 160$ nm, corresponds to a chromospheric rise in temperature starting about 500 km above the height where the disk-center visible continuum is formed. Models based on observations in the extreme ultraviolet (Vernazza, Avrett, and Loeser 1981) indicate that the temperature continues to increase gradually, reaching a value of about 8000 K at a height near 2000 km, where hydrogen begins to be partially ionized and to radiate substantial amounts of energy in the Lyman lines and continuum. Lyman α radiative cooling prevents any further *gradual* temperature rise, but there is enough mechanical heating in these and higher layers to ionize hydrogen completely. These effects cause the atmosphere to have a *transition region* only a few kilometers thick separating the layers where $T = 10^4$ and 10^5 K.

The transition region differs from the chromosphere not only because of its very large temperature and ionization gradients, but also because the radiated energy comes from mechanical energy deposited at higher temperatures and transported downward, rather than from any substantial amount of mechanical energy deposited locally. The transition-region models we discuss here are those of Fontenla, Avrett, and Loeser (1990, 1991, 1992). The temperature distribution in the transition region is not adjusted to match observations, as in the photosphere and chromosphere, but is computed theoretically assuming energy balance, using the boundary conditions near 10^4 K from the chromospheric model, and including the effects of particle diffusion. The downward flow of energy at the 10^5 K boundary is adjusted to balance the radiative energy losses at temperatures between 10^5 and 10^4 K.

In the transition region the upward diffusion of hydrogen atoms causes Lyman α radiation to be emitted at higher temperatures than would occur under conditions of local statistical equilibrium without diffusion. An important transport mechanism in the lower transition region is the recombination energy associated with pairs of protons and electrons that diffuse downward. Differential mass flows also may play a significant role in transporting energy, but we find that assuming hydrostatic equilibrium and accounting for particle diffusion gives computed hydrogen and helium spectra that are consistent with the observations.

The excitation and ionization of He I and He II in the transition region and upper chromosphere are considered in detail by Fontenla *et al.* 1992, hereafter FAL. We find that particle diffusion in the transition region is as important for helium as for hydrogen. In the upper chromosphere the ionization of helium is particularly sensitive to coronal line radiation in the $\lambda < 504$ Å range, while such coronal lines have a much smaller effect on hydrogen.

The He I 10830 Å line is formed almost entirely in the upper chromosphere. The absorption of infrared continuum radiation at 10830 Å by He I $2s\ ^3S$–$2p\ ^3P^0$ transitions at this wavelength depends on the integrated He I $2s\ ^3S$ number density along the line of sight (*i.e.*, on the integrated optical depth of the transition). We show in Section 3 that this integrated optical depth, τ, depends on the strength of

the illuminating coronal radiation, the density at the top of the chromosphere, and the geometrical extent of the upper chromosphere.

2. Model Atmospheres

Before discussing the helium calculations we describe our atmospheric models and comment on their applicability to the inhomogeneous solar atmosphere. As noted earlier the abrupt temperature increase in the transition region occurs where hydrogen first becomes significantly ionized. For a more gradual chromospheric temperature rise than the average one, corresponding to a smaller amount of mechanical heating, the transition region would occur at a greater height. For higher chromospheric temperatures, corresponding to greater mechanical heating, the transition region would be located lower, closer to the photosphere. The calculations indicate, however, only moderate differences in the transition region heights for cell-center, average, and bright-network components of the quiet Sun: 2240, 2200, and 2015 km, respectively. Our plage model has the transition region at a height of 1740 km. Figure 1 shows the temperature distributions for our quiet-Sun component models A (cell-center), C (average), and F (bright network) and for our plage model P. (These atmospheric models are tabulated in FAL.)

Various off-limb observations show evidence of chromospheric and transition-region material at considerably greater heights than indicated in Figure 1. Our hydrostatic models are based on balancing the effects of gravity and hydrostatic pressure, and give the atmospheric stratification in the absence of any dynamical forces that could push the transition region to greater heights in certain areas. An analogous model of the Earth's ocean would be a plane surface, with water below and air above. This one-dimensional model might seem unrealistic to a surfer or to a sailor in a storm, but it would still be a useful model for many purposes.

Our view of how the calculated model stratification may apply to the Sun is indicated in Figure 2 (from FAL). The dark-shaded region is a cross-section of the transition region between the chromosphere and the corona. The height of the transition region may vary irregularly due to dynamical forces not included in our hydrostatic calculation, but over much of the solar surface this height may be close to the hydrostatic value.

Disk spectra obtained near $\mu = 1$ and the temperature distributions determined from them may be insensitive to these irregularities, especially if they occupy a small fraction of the solar surface. However, limb spectra obtained near $\mu = 0$ (*i.e.*, along the horizontal direction in Figure 2) would tend to intersect these high-lying features. Such a horizontal line of sight may be optically thick or optically thin depending on wavelength.

Consider first a wavelength for which a horizontal ray passing above the average height of the transition region becomes optically thick by intersecting only a small number of high-lying features. The ray becomes optically thin only at a still greater height, and the transition region will appear to be located at that height.

Now consider a wavelength for which the optical thickness is of order unity along the ray tangent to the average height of the transition region. The high-lying features are transparent at this wavelength, and the transition region will appear

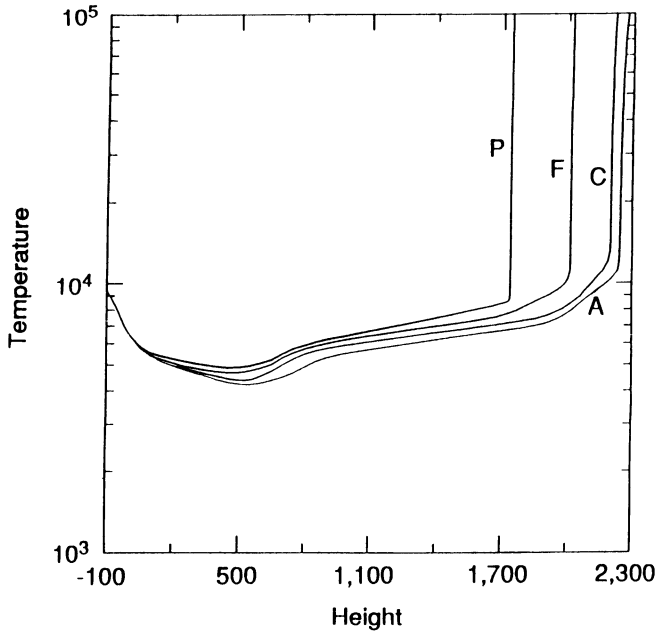

Fig. 1. Temperature (K) vs. height for models A, C, F, and P. Height is in km above the photospheric level where the vertical optical depth is unity in the continuum at 5000 Å.

in this case to be located at its actual average height.

At the center of the 10830 Å line we find that the optical thickness is of order unity along the ray tangent to $h = 2100$ km (where $T \approx 10^4$ K) for model C. Limb observations of this line should therefore be useful in establishing the average height of the transition region. Our calculated off-limb results are shown in Section 5.

3. Model Calculations and Disk Profiles

The properties of the 10830 Å line depend mainly on the density and extent of the upper chromosphere and on the coronal radiation that illuminates this region in the $\lambda < 504$ Å ionizing continuum. Recombination following He I ionization causes the $2s\ ^3S$ level to be populated, and causes $2s\ ^3S$–$2p\ ^3P^0$ absorption of the 10830 Å continuum on the disk.

For the incident radiation we use the observed solar irradiances in the extreme ultraviolet compiled by Tobiska (1991). He lists separate estimates of the irradiance contributions from coronal source regions and from the deeper layers (transition region and chromosphere) differentiated statistically rather than by spatial observations, since they are based on full-disk measurements. Tobiska gives data for times

https://doi.org/10.1017/S0074180900124234 Published online by Cambridge University Press

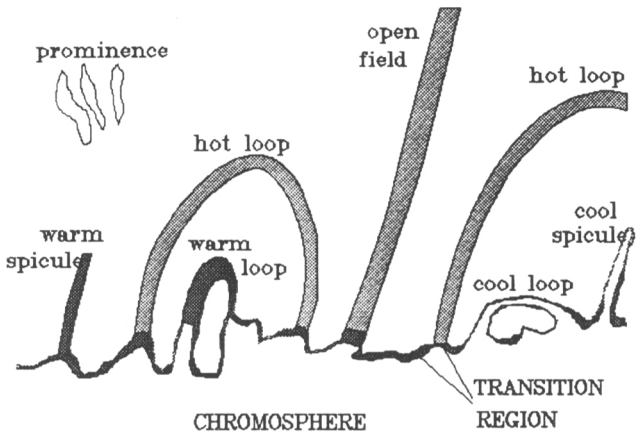

Fig. 2. Some of the magnetic structures observed in the low corona. The sketch indicates cool material (T about 10^4 K) in the chromosphere and in spicules, loops, and prominences; warm material (about 10^5 K) in the transition region and in loops and spicules; and hot material (about 10^6 K) in the loops and open fields.

of low and moderate solar activity, and we have used these results to determine the corresponding mean intensity at the solar surface for coronal source regions only. The results are listed in Table 6 of FAL.

We use the low- and moderate-activity values for our models A and C respectively. For models F and P we use 3 times the moderate activity values. In addition to model C we show the results for models CL and CH which are the same as C except that CL uses the low-activity incident intensities and CH uses the higher values, as in models F and P.

Figure 3 shows the calculated number density of the $2s\ ^3S$ level (in cm^{-3}) as a function of height for models CL, C, and CH. The 10830 line-center optical thicknesses between 1400 and 2200 km in the three cases are 0.042, 0.17, and 0.37, respectively.

The corresponding disk-center absorption lines are shown in Figure 4. The line has three components with relative strengths 0.5556, 0.3333, and 0.1111 at wavelength displacements 0, −0.0898, and −1.249 Å, respectively. The first two are blended together producing a slightly asymmetric result while the third component is well separated. These profiles clearly show the effect of different values of the coronal radiation.

We now consider the relative behavior for models A, C, F, and P. Figure 5 shows the calculated $2s\ ^3S$ number density *vs.* height in each case. The transition region is at a different height for each model. Models CH and F have the same incident

https://doi.org/10.1017/S0074180900124234 Published online by Cambridge University Press

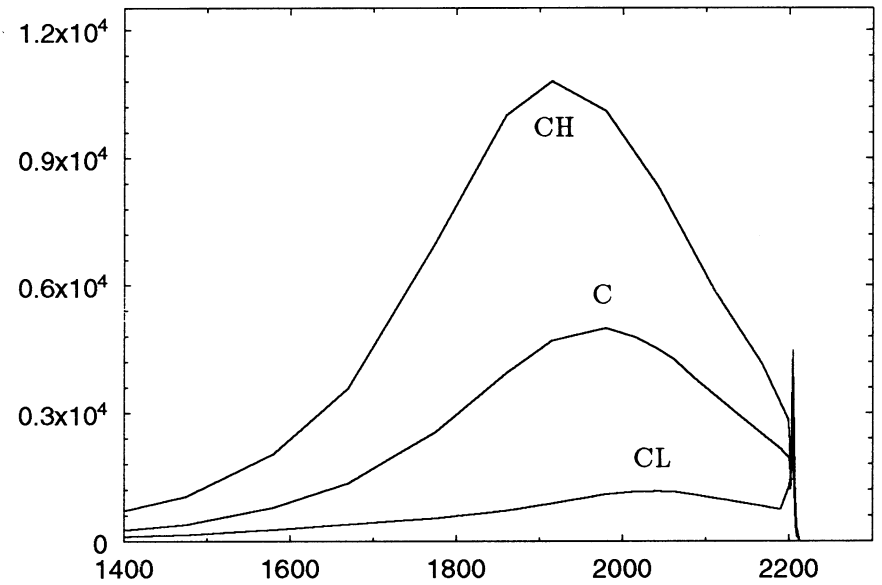

Fig. 3. Number density (cm^{-3}) of the $2s\ ^3S$ level of He I *vs.* height (km) calculated for models CL, C, and CH.

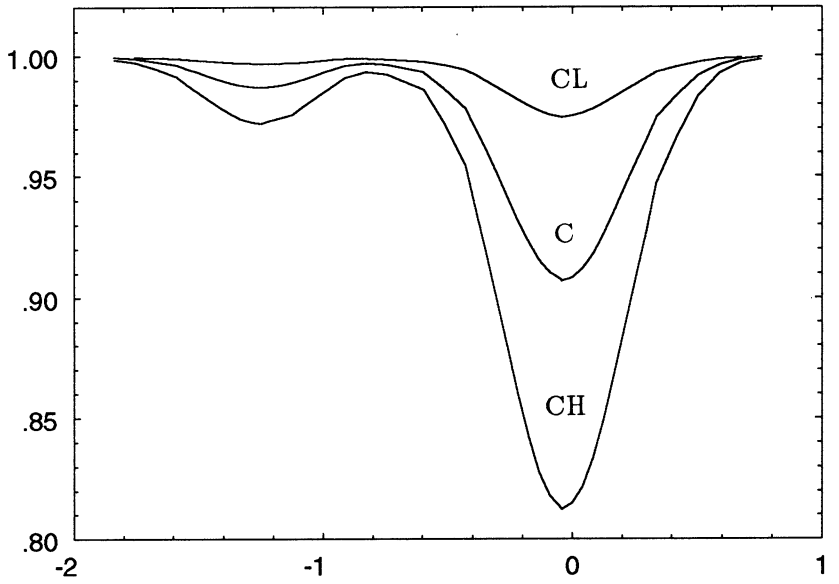

Fig. 4. Disk-center residual intensity of the 10830 Å line *vs.* $\Delta\lambda$ in Å for models CL, C, and CH.

https://doi.org/10.1017/S0074180900124234 Published online by Cambridge University Press

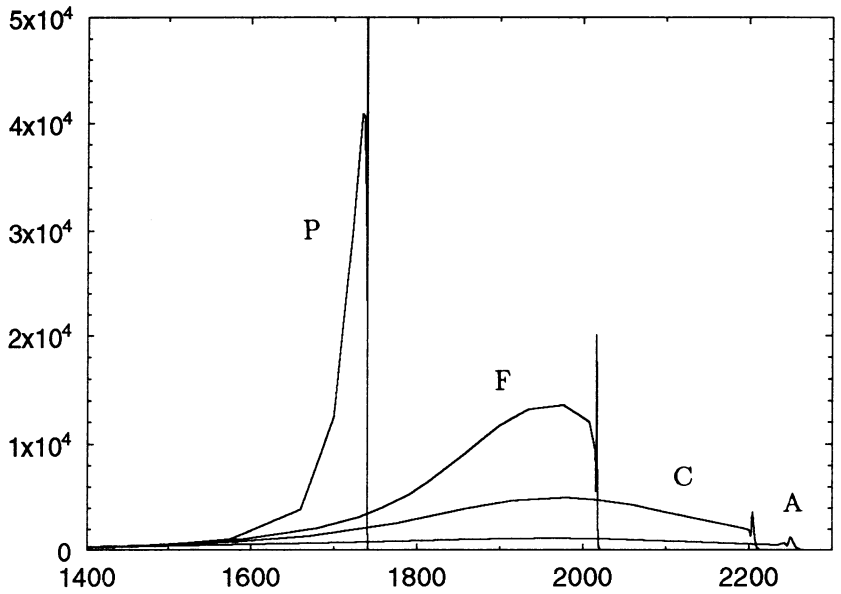

Fig. 5. Number density (cm^{-3}) of the $2s\ ^3S$ level of He I vs. height (km) calculated for models A, C, F, and P.

radiation, and the maximum $2s\ ^3S$ number density is larger for model F than for model CH (see Figure 3), but the integrated model-F number density is smaller because the transition region is located deeper, and because the attenuation of the ionizing $\lambda < 504$ Å radiation in the lower chromosphere is roughly the same in the two cases. The integrated model P number density is less than that of model F for the same reasons. The total line center optical depths for models A, C, F, and P are 0.054, 0.17, 0.26, and 0.15, respectively. The corresponding disk-center profiles are shown in Figure 6. Note that the profile for model P lies between the profiles for models A and C.

These results can be described by the simple equation

$$I_0 = I_c e^{-\tau} + S(1 - e^{-\tau}) \tag{1}$$

where τ is the line center optical thickness of the chromosphere, S is the line source function (which we find to be essentially constant, and equal to about $0.4 \times I_c$), I_c is the continuum intensity at 10830 Å, and I_0 is the line center intensity. In Table I we give the values of these quantities for the various models. The values of I_0/I_c correspond to the residual intensities shown in Figures 4 and 6.

Models A and CL have the same coronal illumination, and the model A chromospheric densities are lower than in model CL, but the chromosphere extends to greater heights in model A. As a result there is slightly more line absorption in the case of model A.

As noted earlier, models CH, F, and P also have the same coronal illumination, and these three models have progressively larger densities at a common location in

https://doi.org/10.1017/S0074180900124234 Published online by Cambridge University Press

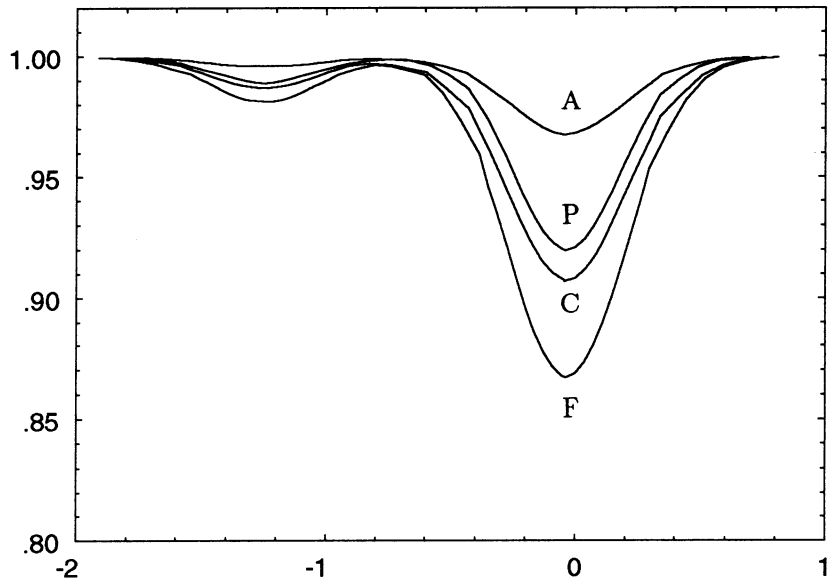

Fig. 6. Disk-center residual intensity of the 10830 Å line vs. $\Delta\lambda$ in Å for models A, C, F, and P.

the chromosphere (at 1700 km for example), but they have progressively smaller amounts of 10830 Å absorption because the geometrical thickness of the chromosphere is progressively smaller, as shown in Figure 5.

The reduction in the height of the transition region (*i.e.*, in the geometrical thickness of the chromosphere) for the brighter component models thus has a substantial effect on the calculated line absorption.

4. Center-to Limb Behavior

From Table I the line center vertical optical thickness of the chromosphere is calculated to be 0.17 for model C. The chromospheric optical thickness increases for disk positions toward the limb, and the line center intensity I_0 decreases relative to the continuum value I_c. The calculated intensity values from center to limb for the six models are listed in Table II.

The values for the fractional radius 1.0 in this table correspond to a line of sight at the limb which is tangent to height $h = 0$, where the vertical optical depth is unity in the continuum at 5000 Å. (We use plane geometry to determine the atmospheric stratification, and then spherical geometry in these intensity calculations.)

5. Calculated Limb Emission

We give the following calculated results at and above the limb: 1) the integrated intensity within a 1 Å band centered on the strongest 10830 Å component, and

https://doi.org/10.1017/S0074180900124234 Published online by Cambridge University Press

TABLE I
Parameters in Equation 1[a]

model	τ	S	I_c	I_0	I_0/I_c
A	0.054	1.6	4.00	3.87	0.968
CL	0.042	1.6	4.01	3.91	0.975
C	0.17	1.6	4.01	3.63	0.905
CH	0.37	1.6	4.01	3.26	0.813
F	0.26	1.7	4.03	3.50	0.868
P	0.15	1.8	4.13	3.80	0.920

[a] S, I_c, and I_0 have the units 10^{-5} ergs cm^{-2} s^{-1} sr^{-1} Hz^{-1}

TABLE II
Line Center (I_0) and Continuum (I_c) Intensities[a] vs. Radial Disk Position

model		fractional radius					
		0	0.5	0.8	0.9	0.95	1.0
A	I_0	3.87	3.70	3.32	3.02	2.76	1.78
	I_c	4.00	3.84	3.49	3.21	2.98	2.04
	I_0/I_c	0.97	0.96	0.95	0.94	0.93	0.87
CL	I_0	3.91	3.75	3.38	3.09	2.82	1.88
	I_c	4.01	3.85	3.50	3.23	3.00	2.12
	I_0/I_c	0.98	0.97	0.97	0.96	0.94	0.89
C	I_0	3.63	3.45	3.02	2.72	2.43	1.63
	I_c	4.01	3.85	3.50	3.23	3.00	2.12
	I_0/I_c	0.91	0.90	0.87	0.84	0.81	0.77
CH	I_0	3.26	3.06	2.63	2.30	2.04	1.49
	I_c	4.01	3.85	3.50	3.23	3.00	2.12
	I_0/I_c	0.81	0.79	0.75	0.71	0.68	0.70
F	I_0	3.50	3.32	2.89	2.57	2.30	1.60
	I_c	4.03	3.87	3.53	3.27	3.06	2.26
	I_0/I_c	0.87	0.86	0.82	0.79	0.75	0.71
P	I_0	3.80	3.63	3.25	2.95	2.69	1.80
	I_c	4.13	3.98	3.66	3.42	3.23	2.50
	I_0/I_c	0.92	0.91	0.89	0.86	0.83	0.72

[a] in 10^{-5} ergs cm^{-2} s^{-1} sr^{-1} Hz^{-1}

https://doi.org/10.1017/S0074180900124234 Published online by Cambridge University Press

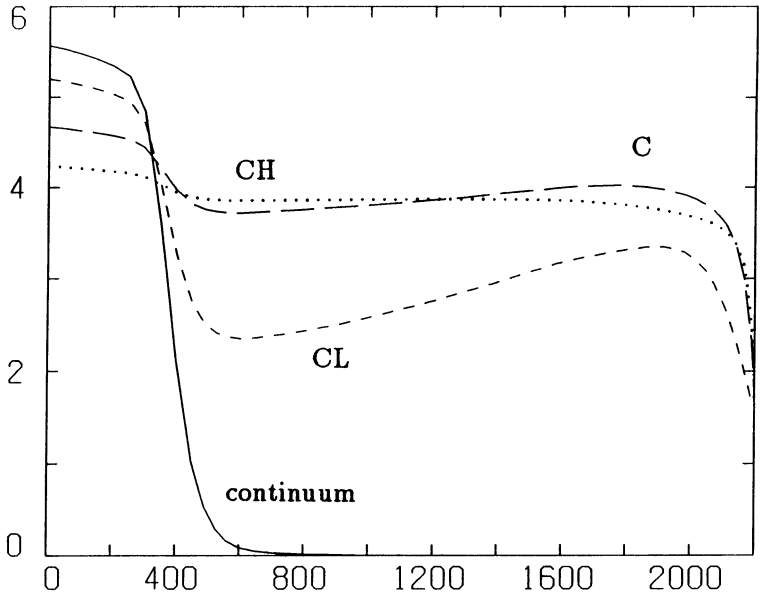

Fig. 7. Off-limb intensity in 10^5 ergs cm^{-2} s^{-1} sr^{-1} within a 1 Å pass-band centered on the strongest component of the 10830 Å line vs. tangential height above the photosphere in km, for models CL (short dashes), C (long dashes), and CH (dots). The solid curve shows the corresponding intensity in the nearby continuum within a 1 Å pass-band.

2) the integrated intensity within a nearby 1 Å continuum band. For simplicity these will be called line and continuum intensities, respectively. Figure 7 shows the off-limb intensities for models CL, C, and CM plotted *vs.* tangential height h (defined above). The continuum intensity, which is the same for the three models, exceeds the line intensity at $h = 0$ but then decreases rapidly with height as the continuum becomes transparent. The chromosphere has a line optical thickness of order unity along the limb tangent ray and becomes optically thick as the tangent height increases. The chromosphere becomes optically thin again only for rays tangent to the top of the chromosphere and above. The curves corresponding to models C and CH in Figure 7 are similar because in these two cases the chromosphere is optically thick along rays tangent to heights in the range 500–2000 km, while the model CL line intensity shows a lower minimum value because the low chromosphere is more transparent.

6. Off-Limb Observations

We are not aware of any published observations that can be compared directly with the results in Figure 7. However, the 10830 Å line is very similar to, but stronger than, the He I D_3 line at 5875.68 Å. (The 10830 and D_3 transitions take place between the levels $2s\ ^3S$–$2p\ ^3P^0$ and $2p\ ^3P^0$–$3d\ ^3D$, respectively.) The observed brightness distribution above the limb is reported to be very similar for the two lines

https://doi.org/10.1017/S0074180900124234 Published online by Cambridge University Press

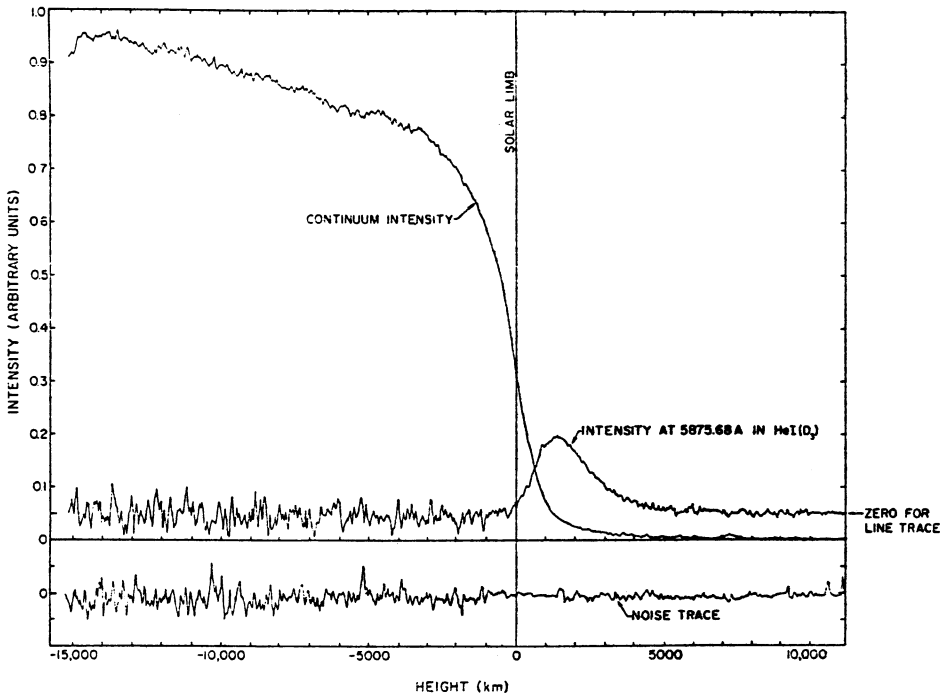

Fig. 8. Residual intensity *vs.* height above the limb in the He I D_3 line at 5875.68 Å obtained by subtracting the continuum variation at the limb from that in the line. The continuum variation and a residual noise trace are shown for reference. No seeing corrections were made in the data shown. From White (1963).

(S. Koutchmy, private communication). Both show emission above the limb that extends to $h \approx 2000$ km, the height of the upper chromosphere in the hydrostatic models.

Figure 8 shows the D_3 emission above the limb measured by White (1963). The residual line emission shown in this figure is obtained by subtracting the corresponding continuum intensity in the same narrow bandwidth used for the line. The continuum distribution is plotted for reference. There is essentially no D_3 absorption on the disk, so that subtracting the continuum gives a good measure of the line emission corrected for the effects of scattered light. Since the line-center 10830 intensity is less than the continuum value on the disk, subtracting the continuum would cause negative residual values for $h < 300$ km.

Eclipse observations of the D_3 line have been reported by Athay and Menzel (1956), Gulyaev (1971,1972), and Lifshitz *et al.* (1976). Zirin (1975) published filtergrams showing D_3 emission above the limb at a level of about 10% of the central disk intensity. He found the emission to be reduced by a factor of 2 to 3 in coronal holes. Koutchmy and Avrett (1989) reported similar results based on observations

https://doi.org/10.1017/S0074180900124234 Published online by Cambridge University Press

by Koutchmy at Sacramento Peak Observatory: the D_3 emission has a maximum at a height of about $h = 1800$ km except in coronal holes where there is little extended emission above the limb.

In Sections 3 and 4 of this paper we have shown the calculated behavior of the 10830 Å line on the disk, but we have not attempted to compare these results with observations. He I 10830 Å observations are discussed in the papers of Jones (1993), Fleck *et al.* (1993), Harvey and Livingston (1993), and Harvey (1993) in these proceedings.

7. Conclusions

Our model calculations indicate that the line absorption clearly depends on the coronal illumination. However, the computed profiles corresponding to different spatial components of the atmosphere also depend on the geometrical thickness of the upper chromosphere and on the density of this region.

We give results based on one-dimensional hydrostatic-equilibrium models of faint, average, and bright components of the quiet Sun and of a plage region. In these four cases the transition region is located at successively lower heights, *i.e.*, the chromosphere is successively reduced in extent. From a theoretical viewpoint the only way to avoid this effect is for the brighter component models to be subject to successively larger dynamic or Lorentz force contributions, in order to increase their chromospheric scale heights.

A consequence of the decrease in chromospheric thickness, despite the increase in density at the top of the chromosphere, is a decrease in 10830 absorption. It should be possible to use observations at other wavelengths to distinguish between 1) this decrease in 10830 absorption in regions that are brighter at other wavelengths due to chromospheric heating, and 2) the decrease due to diminished EUV coronal illumination.

In our model calculations we arbitrarily chose the coronal illumination for model F and for model P to be 3 times that of model C. We found the 10830 line for model P to be weaker than that of model C because of the reduced geometrical thickness of the chromosphere in the model P calculation. Since observations of plage regions show more absorption at 10830 Å than do observations of quiet regions, the model P calculation discussed here needs to be modified either by increasing the chromospheric scale heights in some way, or by increasing the coronal illumination. We believe that an increase in illumination is the change that is primarily needed.

It would be useful to have quantitative off-limb measurements of the 10830 Å line to compare with the results in Figure 7. We expect such observations to resemble those of the similar but weaker D_3 line: to show emission that extends out to roughly 2000 km, as in Figure 7, and that weakens in coronal hole regions. The observed intensity distribution is not expected to have the sharp drop-off at 2200 km shown in Figure 7, but to have a more gradual decrease (as in Figure 8) corresponding to the fraction of chromospheric and transition-region material located at greater heights.

Acknowledgements

This research was supported by NASA grants NSG-7054 and NAGW-2096.

References

Athay, R. G., and Menzel, D. H.: 1956, *Astrophys. J.* **123**, 285.
Fleck, B., Deubner, F. -L., Maier, D., and Schmidt, W.: 1993, these proceedings.
Fontenla, J. M., Avrett, E. H., and Loeser, R.: 1990, *Astrophys. J.* **355**, 700.
Fontenla, J. M., Avrett, E. H., and Loeser, R.: 1991, *Astrophys. J.* **377**, 712.
Fontenla, J. M., Avrett, E. H., and Loeser, R.: 1992, *Astrophys. J.* in press.
Gulyaev, R. A.: 1971, *Solar Phys.* **18**, 410.
Gulyaev, R. A.: 1972, *Solar Phys.* **24**, 72,
Harvey, J., and Livingston, W.: 1993, these proceedings.
Harvey, K.: 1993, these proceedings.
Jones, H. P.: 1993, these proceedings.
Koutchmy, S., and Avrett, E. H.: 1989, unpublished conference manuscript available from the authors.
Lifshits, M. A., Akimov, L. A., Belkina, I. L., and Dyatel, N. P.: 1976, *Solar Phys.* **49**, 315.
Tobiska, W. K.: 1991, *J. Atmos. Terr. Phys.*, **53**, 1005.
Vernazza, J. E., Avrett, E. H., and Loeser, R.: 1991, *Astrophys. J. Suppl.* **45**, 635.
White, O. R.: 1963, *Astrophys. J.* **138**, 1316.
Zirin, H.: 1975, *Astrophys. J.* **199**, L63.